Published in final edited form as:
J Nucl Med. 2014 January ; 55(1): 154–160. doi:10.2967/jnumed.113.122069.

^{18}F-Alfatide II and ^{18}F-FDG Dual Tracer Dynamic PET for Parametric, Early Prediction of Tumor Response to Therapy

Jinxia Guo[1,2,3,*], **Ning Guo**[2,4,*], **Lixin Lang**[2], **Dale O. Kiesewetter**[2], **Qingguo Xie**[1], **Quanzheng Li**[4], **Henry S. Eden**[5], **Gang Niu**[2], and **Xiaoyuan Chen**[2]

[1]Department of Biomedical Engineering and Wuhan National Laboratory for Optoelectronics (WNLO), Huazhong University of Science and Technology, Wuhan, Hubei, China [2]Laboratory of Molecular Imaging and Nanomedicine (LOMIN), National Institute of Biomedical Imaging and Bioengineering, National Institutes of Health (NIBIB), Bethesda, Maryland [3]Center for Molecular Imaging and Translational Medicine (CMITM), School of Public Health, Xiamen University, Xiamen, China [4]Center for Advanced Medical Imaging Science, Department of Radiology, Massachusetts General Hospital, Harvard Medical School, Cambridge, MA [5]Intramural Research Program (IRP), National Institute of Biomedical Imaging and Bioengineering, National Institutes of Health (NIBIB), Bethesda, Maryland

Abstract

A single dynamic PET acquisition using multiple tracers administered closely in time could provide valuable complementary information about a tumor's status under quasi-constant conditions. This study aims to investigate the utility of dual-tracer dynamic PET imaging with ^{18}F-Alfatide II (^{18}F-AlF-NOTA-E[PEG$_4$-c(RGDfk)]$_2$) and ^{18}F-FDG for parametric monitoring of tumor responses to therapy.

Methods—We administered doxorubicin to one group of athymic nude mice with U87MG tumors and Abraxane to another group of mice with MDA-MB-435 tumors. To monitor therapeutic responses, we performed dual-tracer dynamic imaging, in sessions that lasted 90 min, starting by injecting the mice *via* tail vein catheters with ^{18}F-Alfatide II, followed 40 minutes later by ^{18}F-FDG. To achieve signal separation of the two tracers, we fit a three-compartment reversible model to the time activity curve (TAC) of ^{18}F-Alfatide II for the 40 min prior to ^{18}F-FDG injection, and then extrapolated to 90 min. The ^{18}F-FDG tumor TAC was isolated from the 90 min dual tracer tumor TAC by subtracting the fitted ^{18}F-Alfatide II tumor TAC. With separated tumor TACs, the ^{18}F-Alfatide II binding potential ($Bp=k_3/k_4$) and volume of distribution (V_D), and ^{18}F-FDG influx rate ($((K_1\times k_3)/(k_2 + k_3))$) based on the Patlak method were calculated to validate the signal recovery in a comparison with 60-min single tracer imaging and to monitor therapeutic response.

Results—The transport and binding rate parameters K_1-k_3 of ^{18}F-Alfatide II, calculated from the first 40 min of dual tracer dynamic scan, as well as Bp and V_D, correlated well with the

For correspondence or reprints contact the following: Xiaoyuan Chen, Ph.D., 31 Center Drive, Suite 1C14, Bethesda, MD 20892-2281, shawn.chen@nih.gov Or Gang Niu, Ph.D., 10 Center Drive, 10/B3B25, Bethesda, MD 20892-2281, niug@mail.nih.gov.
Jinxia Guo and Ning Guo contributed equally.

parameters from the 60 min single tracer scan ($R^2 > 0.95$). Compared with the results of single tracer PET imaging, FDG tumor uptake and influx were recovered well from dual tracer imaging. Upon doxorubicin treatment, while no significant changes in static tracer uptake values of ^{18}F-Alfatide II or ^{18}F-FDG were observed, both ^{18}F-Alfatide II Bp and ^{18}F-FDG influx from kinetic analysis in tumors showed significant decreases. For Abraxane therapy of MDA-MB-435 tumors, significant decrease was only observed with ^{18}F-Alfatide II Bp value from kinetic analysis but not ^{18}F-FDG influx.

Conclusion—The parameters fitted with compartmental modeling from the dual tracer dynamic imaging are consistent with those from single tracer imaging, substantiating the feasibility of this methodology. Even though no significant differences in tumor size were found until 5 days after doxorubicin treatment started, at day 3 there were already substantial differences in ^{18}F-Alfatide II Bp and ^{18}F-FDG influx rate. Dual tracer imaging can measure ^{18}F-Alfatide II Bp value and ^{18}F-FDG influx simultaneously to evaluate tumor angiogenesis and metabolism. Such changes are known to precede anatomical changes, and thus parametric imaging may offer the promise of early prediction of therapy response.

Keywords

dual-tracer dynamic PET; parametric imaging; ^{18}F-Alfatide II; ^{18}F-FDG; therapy response

Positron emission tomography (PET) is arguably the most sensitive and specific technique for imaging molecular pathways *in vivo* in humans. Moreover, the availability of tracers sensitive to different physiological and pharmacological variables enables PET to characterize multiple aspects of oncologic pathology, including metabolism, angiogenesis, cellular proliferation, blood flow and hypoxia (1, 2). Given the complexity and heterogeneity of malignant lesions, such complementary information can facilitate comprehensive evaluation of tumors, and improve early detection, staging, and monitoring of therapeutic responses (3–7).

For example, Tseng *et al.* (5) concurrently measured blood flow with ^{15}O-water and glucose metabolism with ^{18}F-FDG in locally advanced breast cancer, and reported that a low ratio of glucose metabolism to blood flow predicted a favorable therapeutic response. In our previous studies, we employed ^{18}F-FPPRGD2, a peptide that quantifies integrin $\alpha_v\beta_3$ expression, and ^{18}F-FDG to evaluate tumor angiogenesis and metabolism modulations in response to the VEGFRTK inhibitor ZD4190 (7), to Abraxane (6), and to the vascular disruptive fusion protein $VEGF_{121}$/rGel (8). Longitudinal imaging results indicated that even though much higher tumor uptake was found in ^{18}F-FDG imaging, therapeutic effect was more clearly reflected by ^{18}F-FPPRGD2 imaging. However, the multiple-step synthetic procedure required to prepare ^{18}F-FPPRGD2 with relatively low yield may limit its widespread use (9). Consequently, a novel dimeric RGD peptide tracer has been prepared with the reaction of ^{18}F-aluminum-fluoride complex to pre-attached chelator on RGD peptides (10). Without the need of HPLC purification, the ease of preparation and high imaging qualities make ^{18}F-AlF-NOTA-$PRGD_2$ a promising alternative to ^{18}F-$FPPRGD_2$ for PET imaging of $\alpha_v\beta_3$ integrin expression (10–12).

By taking advantage of the distinct kinetics of different tracers, nearly simultaneous multi-tracer imaging can be achieved by closely staggering tracer injections during a single scan (13–17). Many studies using simulated data have demonstrated the feasibility of signal separation with dual tracer dynamic PET imaging (13–17). PET imaging with different tracers that partially overlap in time has advantages, relative to PET imaging with widely separated administration of the tracers, by reducing the cost and time of the imaging, and by providing complementary information under quasi-constant physiological conditions (14, 18). Dynamic parameters for each tracer may provide more sensitive quantification in tumor therapy monitoring than static tumor uptake values (19). In addition, the radiation dose is reduced in multi-tracer single-scan imaging, because only one CT scan is needed for attenuation correction and/or co-registration of images for the tracers.

Dynamic PET imaging using ^{18}F-FDG, followed by irreversible compartmental modeling, has been intensively studied (5). Our previous studies showed that the kinetics of RGD-based peptide tracer satisfies the reversible three-compartment model (19). In this study, we conducted dynamic imaging with dual tracers ^{18}F-AlF-NOTA-E[PEG$_4$-c(RGDfk)]$_2$ (denoted as ^{18}F-Alfatide II) (20) and ^{18}F-FDG in xenograft tumor models to monitor tumor therapy response to either doxorubicin or Abraxane. ^{18}F-Alfatide II and ^{18}F-FDG tumor time-activity curves (TACs) were separated by using compartmental modeling. To validate the signal recovery, the dynamic parameters calculated from dual tracer TACs were compared with those from single tracer imaging. Then the tumor response to drug treatment was assessed based on tumor uptake, ^{18}F-Alfatide II Bp, and ^{18}F-FDG influx rate (5, 6).

MATERIALS AND METHODS

Preparation of the Imaging Tracers

The PEG$_4$-E[c(RGDfK)$_2$] was synthesized by C S Bio (Menlo Park, CA). The NOTA-NHS ester was obtained from CheMatech (Dijon, France). The coupling of NOTA-NHS ester to the amine of RGD peptide was performed using dimethylformamide (DMF) as the solvent and *N*,*N*-diisopropylethylamine(DIPEA) as the base. The purity of NOTA-PEG$_4$-E[c(RGDfK)$_2$] was > 97% by analytical HPLC (Rt = 14.2 min) running a linear gradient starting from 5% A (0.1% TFA in acetonitrile) and 95% B (0.1% TFA in water) for 5 min and increasing to 65% A at 35 min with a flow rate of 1 ml/min. The reaction yield was 69%. LC-MS: $[MH]^+$= 1850.7869 (m/z), calc: 1849.9322 ($C_{82}H_{127}N_{23}O_{26}$).

The ^{18}F-fluoride in O-18 water was obtained from the NIH cyclotron facility. The radiolabeling of NOTA-PEG$_4$-E[c(RGDfK)$_2$] with ^{18}F-aluminum fluoride was performed according to a previously published procedure with some modifications (21). The total synthesis time was about 30 min with radiochemical yield of 40–60% and radiochemical purity > 95%. The specific activity was about 14.8–37 GBq/μmol at the end of synthesis based on the amount of peptide used and the amount of radioactivity trapped on the C-18 column. The final product was named ^{18}F-Alfatide II (^{18}F-AlF-NOTA-E[PEG$_4$-c(RGDfk)]$_2$). ^{18}F-FDG was purchased from the Nuclear Pharmacy of Cardinal Health and was diluted, as appropriate, with sterile saline.

Tumor Model and Treatment Protocol

All animal studies were conducted in accordance with the principles and procedures outlined in the Guide for the Care and Use of Laboratory Animals and were approved by the Institutional Animal Care and Use Committee of the Clinical Center, NIH. The U87MG cells expressing high level of $\alpha_v\beta_3$ integrin (22) and the MDA-MB-435 cells with medium level of $\alpha_v\beta_3$ integrin expression were purchased from the American Type Culture Collection (ATCC) and cultured in MEM and Leibovitz's L-15 medium supplemented with 10% fetal bovine serum in a humidified atmosphere of 5% CO_2 at 37°C, respectively. The tumor models were established by inoculating the right shoulder of 5- to 6-week old female athymic nude mice (Harlan Laboratories) subcutaneously with 1×10^7 U87MG cells or 6×10^6 MDA-MB-435 cells in 100 μl PBS. The mice underwent PET scans when the tumor volume reached 200–400 mm^3 (about 3~4 weeks after inoculation). For the therapy monitoring study, U87MG tumor-bearing mice in the treated group were given two doses of doxorubicin (5 mg/kg/dose) two days apart *via* tail vein injection, while the MDA-MB-435 tumor-bearing mice were given two doses of Abraxane (30 mg/kg/dose) every other day *via* tail vein injection. All the mice in the control group were injected with the same volume of saline. The detailed therapy and imaging regimen was shown in Table 1. Tumor growth was monitored by measuring tumor size with a caliper every 2 days after the tumors became palpable. The tumor volume was calculated with the formula $a\times(b^2)/2$, where a and b were the tumor length and width, respectively, in mm.

Dynamic PET Imaging

All the PET scans were conducted with an Inveon small-animal PET scanner (Siemens Preclinical Solution). Mice were anesthetized with mixtures of 1 ml/min O_2 and 1.5% isoflurane and kept warm with a heating pad thermostat during the imaging. All data acquisitions were initiated immediately before the tracer injections. The duration of a scan was 60 min for single tracer imaging and 90 min for ^{18}F-Alfatide II/^{18}F-FDG dual tracer imaging. A catheter was placed in the tail vein before each scan for tracer administration. For dual tracer imaging, about 3.7 MBq of ^{18}F-Alfatide II was injected through the catheter immediately after the scan was started. Forty minutes later, about 3.7 MBq of ^{18}F-FDG was injected without stopping the scanning. For therapy response monitoring, mice in both control and treated groups underwent dual tracer dynamic imaging on day 0 and day 3. The acquired list mode data were reconstructed with 3D-OSEM followed by the MAP algorithm (11). The reconstruction frames were 1×5s, 1×25s, 9×30s, 5×60s, 5×120s and 10×240s for single tracer dynamic imaging and 1×5s, 1×25s, 9×30s, 10×60s, 4×300s, 1×240s, 12×30s, 10×60s, 7×300s for dual tracer dynamic imaging.

ROI Quantification and Time Activity Curves

The regions of interest (ROIs) were drawn over the tumor region using Inveon Research Workplace (IRW) 3.0 software (Siemens Preclinical Solution), using a procedure reported in our previous study (11). For dual tracer dynamic imaging, the TACs were generated based on mean pixel intensity of the whole ROI in each frame before the signal separation. A calibration constant was used to convert the mean pixel intensity to μCi/ml for separated TACs. As the tissue density was assumed to be 1 g/ml, the activity in ROI was normalized

by injected dose and expressed as percent injected dose per gram (%ID/g) to describe the tissue uptake of the radiotracers. The injected dose for the second tracer, ^{18}F-FDG, was decay-corrected to the starting time of the scanning to reflect the real tumor uptake. The tumor uptake of ^{18}F-Alfatide II in static image quantification was calculated from the last frame before ^{18}F-FDG injection. ^{18}F-FDG uptake was calculated at the 50min time point on the restored ^{18}F-FDG TACs.

The arterial input function was drawn on the abdominal aorta (23) on the second frame of PET dynamic image serials. The first frame was left empty purposely to make sure the peak concentration could be captured.

Dual Tracer Input Function and Tumor TAC Separation

The ^{18}F-Alfatide II input function was fitted with a tri-exponential model (24) for the first 40 min of data. The mathematical expression for the model is shown in Eq. 1

$$C_p=\sum_{i=1}^{3}A_i \bullet \exp(-\lambda_i \bullet (t-\tau)) \quad t \geq \tau \quad (1)$$

Where C_p represents the tracer concentration in plasma. A_1, A_2 and A_3 are coefficients of the model and λ_1, λ_2 and λ_3 are the eigen values of the model. τ is the injection delay time.

For tumor TAC separation, three-compartment reversible model was used to fit the initial 40 min of ^{18}F-Alfatide II data. The dynamic rate constants K_1-k_4 were determined by fitting the following function for tumor TAC.

$$C_t=\frac{K_1}{\alpha_2-\alpha_1}[(k_3+k_4-\alpha_1)\,\mathrm{e}^{-\alpha_1 t}+(\alpha_2-k_3-k_4)\,\mathrm{e}^{-\alpha_2 t}] \otimes C_p+V_b C_p \quad (2.1)$$

$$\alpha_1=\frac{(k_2+k_3+k_4)-\sqrt{(k_2+k_3+k_4)^2-4k_2k_4}}{2} \quad (2.2)$$

$$\alpha_2=\frac{(k_2+k_3+k_4)+\sqrt{(k_2+k_3+k_4)^2-4k_2k_4}}{2} \quad (2.3)$$

Here C_t is the tracer concentration in tumor ROI and V_b is the fractional blood volume.

Similarly, K_1-k_4 were then imported back into the Eq. 2.1–2.3 to extrapolate the ^{18}F-Alfatide II TAC to 90 min. Subsequently, the ^{18}F-FDG tumor TAC was restored by subtracting the fitted 90 min ^{18}F-Alfatide II TAC from the overlapping TAC in the dual tracer imaging.

The fitting method for the input function and the tumor TACs, alike, was unweighted least squares nonlinear regression. The correlation coefficient R^2, defined as the ratio of

regression sum of squares (RSS) and the total sum of squares (TSS), was calculated to evaluate the goodness of fit (25).

Kinetic Data Analysis

The combination binding potential ($Bp=k_3/k_4$) and volume of distribution ($V_D=(K_1/k_2)\times(1+k_3/k_4)$) were calculated, in addition to K_1-k_4, for ^{18}F-Alfatide II. Bp is associated with the binding affinity and V_D reflects the tissue-to-plasma concentration ratio. The Patlak method was performed to calculate the influx rate constant for ^{18}F-FDG, a well-known irreversible tracer. The influx rate is related to the metabolic rate of glucose (MRglu) (26).

Logan graphical analysis (19) was used in the therapeutic monitoring study to calculate a voxel-wise parametric map of ^{18}F-Alfatide II Bp values, using data from the dynamic whole body images obtained during the first 40 min of the study, i.e., before injection of ^{18}F-FDG.

Statistics

Linear regression was used to compare the results from single tracer and dual tracer imaging and evaluated by ANOVA *F* test to validate the significance of regression, with a P value of < 0.05 indicating significant linearity. For therapeutic monitoring, quantitative data were expressed as mean ± SD. Means were compared using Student's t test. A P value of < 0.05 was considered statistically significant.

RESULTS

Time Activity Curves and Dual Tracer TAC Separation

After dynamic acquisition and imaging reconstruction, ROIs were drawn over the abdominal aorta and tumor region to generate the corresponding dual tracer TACs (Supplementary Figure 1). In order to evaluate the robustness of the non-linear regression, a regression coefficient of each animal was calculated, and listed in Table 2. R^2 ranged from 0.92 to 1.0, indicating a good fit for all.

Average U87MG tumor uptake TACs were calculated and are shown in Figure 1A for ^{18}F-Alfatide II and Figure 1B for ^{18}F-FDG, respectively. In the dual tracer imaging study the tumor uptake of ^{18}F-Alfatide II was 4.65 ± 1.02 %ID/g at 40 min and the uptake of ^{18}F-FDG was 11.31 ± 1.61 %ID/g at 50 min. In the single tracer imaging study the tumor uptake of ^{18}F-Alfatide II was 4.38 ± 1.43 %ID/g at 40 min and the uptake of ^{18}F-FDG was 10.81 ± 0.81 %ID/g at 50 min. There is no significant difference between the values calculated from the single tracer imaging and dual tracer imaging. Similarly, the average MDA-MB-435 tumor uptake TACs from the dual tracer imaging fitted very well with that from the single tracer imaging (Figure 1C & D). The MDA-MB-435 tumor uptake values of ^{18}F-FDG and ^{18}F-Alfatide II from the dual tracer imaging were 7.19 ± 1.31 and 2.79 ± 0.47 %ID/g respectively and showed no significant difference with those from the single tracer imaging (6.96 ± 1.13 and 2.73 ± 0.64 %ID/g respectively).

Kinetic Parameters Evaluation

^{18}F-Alfatide II kinetic parameters, such as K_1, k_2 and k_3, calculated from the 40 min and 60 min dynamic scans showed excellent linear correlation ($R^2 > 0.98$), while k_4 showed modest (but still statistically significant, $P < 0.05$) correlation ($R^2 = 0.76$) (Supplementary Figure 2). Excellent linear correlations were also found for V_D ($R^2 = 0.95$) and Bp ($R^2 = 0.98$), indicating V_D and Bp derived from the 40 min scan were very consistent with the ones derived from the 60 min scan (Figure 2A & B).

Kinetic parameter comparisons for ^{18}F-FDG between single and dual tracer imaging are shown in Figure 2C & D. The correlation coefficients, R^2, for tumor influx and uptake between single tracer and dual tracer imaging were 0.70 and 0.79, respectively. Significant linear correlation was also observed between these parameters ($P < 0.05$), confirming the feasibility of the signal separation and parameter calculations.

Evaluation of Tumor Response to Doxorubicin and Abraxane

After being treated with two doses of doxorubicin, the U87MG tumors showed a partial response, reflected by significant growth inhibition at day 5 after the treatment started ($P < 0.05$, Figure 3A). Tumors in representative static images at 40 min and 90 min time points clearly had heterogeneous tracer distribution within the tumor region in both control and treated groups. The parametric maps of ^{18}F-Alfatide II Bp value were also calculated and are shown in Figure 3B.

Through specific binding to integrin $\alpha_v\beta_3$, ^{18}F-Alfatide II was used to evaluate tumor angiogenesis. In untreated tumors, tumor uptake at 40 min p.i. showed a slight increase with a day-3 to day-0 ratio of 1.18 ± 0.36. Upon treatment, the tumor uptake of ^{18}F-Alfatide II decreased with a day-3 to day-0 ratio of 0.86 ± 0.15. However, the static tumor uptake ratio showed no significant difference between the control and treated groups at 40 min p.i. ($P > 0.05$). The Bp value increased substantially from day 0 to day 3 in the control group, but decreased dramatically in the treated group. Consequently, the day-3 to day-0 Bp ratio of the control group (1.64 ± 0.02) is significantly higher than that of the treated group (0.53 ± 0.14, $P < 0.01$) (Figure 3C).

The tumor uptake of ^{18}F-FDG on day 3 decreased slightly over day 0 in both the control and treated groups (Figure 3C), and to a greater extent in the treated group. Specifically, the day-3 to day-0 ratio of ^{18}F-FDG tumor uptake was 0.95 ± 0.17 for the control group and 0.80 ± 0.16 for the treated group. However, the difference was not statistically significant ($P > 0.05$). ^{18}F-FDG influx rate decreased in both the control and treated groups at day 3 (Figure 3C). The day-3 to day-0 ratio of influx rate was 0.79 ± 0.03 for the control group, which was significantly different from that for the treated group (0.54 ± 0.14, $P < 0.05$).

Treatment with Abraxane also induced a partial response on MDA-MB-435 tumors, reflected by significant growth inhibition at day 4 after the treatment started ($P < 0.05$, Figure 4A). As shown in Figure 4B, both treated and control tumors showed positive uptake of ^{18}F-Alfatide II and ^{18}F-FDG. Similar with doxorubicin treated U87MG tumors, the static tumor uptake ratio of both ^{18}F-Alfatide II and ^{18}F-FDG showed no significant difference between the control and treated groups ($P > 0.05$) (Figure 4C). The day-3 to day-0 ratio

of ^{18}F-FDG influx rate was 0.85 ± 0.17 for the control group, which was not significantly different from that for the treated group (0.80 ± 0.24, $P > 0.05$). The day-3 to day-0 Bp ratio of the treated group (0.66 ± 0.12) is significantly lower than that of the control group (0.97 ± 0.09, $P < 0.01$) (Figure 4C).

DISCUSSION

PET imaging using multiple tracers is expected to provide more complementary information than a single PET study using a single tracer, and thus might improve tumor diagnosis and therapeutic monitoring. Multiple, separate single-tracer studies to achieve this would be more costly and require longer total scan times, and—because of the delay between scans—wouldn't provide information under quasi-consistent physiological conditions.

The fixed-energy gamma ray of positron emitters from the positron-electron annihilation, however, presents significant challenges for imaging multiple tracers simultaneously with one PET scan. Since the 1980s, several methods have been developed to separate the superimposed PET signals of multiple tracer scan (16, 27). For example, Koeppe *et al*. (16) performed computer simulations and human PET studies using pairs of ^{11}C labeled tracers in a single scan to image different neurotransmitter-neuroreceptor systems, and demonstrated the feasibility of parameter estimation with compartmental modeling. Rust *et al*. (17) demonstrated the influence of injection timing, injection order and relative dose on signal separation based on simulated TACs after staggered injection of ^{62}Cu-PTSM and ^{62}Cu-ATSM. Short half-life isotopes, such as ^{11}C ($t_{1/2}$ = 20.4 min), ^{13}N ($t_{1/2}$ = 9.97 min) and ^{62}Cu ($t_{1/2}$ = 9.7 min), were mainly used in these studies to reduce the staggering time between tracer injection and the signal overlap. However, the accuracy of dynamic parameters estimation could be affected due to the limited detectable counts.

With a half-life of 109.8 min, F-18 is the most widely used positron emitting radioisotope for PET imaging. Most recently, Kadrmas *et al.* (28) simulated single scan dual-tracer ^{18}F-FLT/^{18}F-FDG PET imaging, characterizing the performance of recovered static and dynamic imaging measures for each tracer from dual-tracer datasets. In the current study, we conducted ^{18}F-Alfatide II and ^{18}F-FDG dual tracer dynamic imaging in one scan with a 40 min injection separation. After validating the data acquisition and analysis, we successfully applied this strategy to evaluate the tumor response to drug treatment.

The performance of signal separation with overlapping data in dual tracer imaging is affected mainly by tracer injection order, the dose of each tracer, and the injection delay. In our previous RGD kinetics analysis studies, RGD tracers showed fast circulation clearance and urinary excretion (6, 7, 9). In addition, RGD disposition was not affected by factors such as mouse blood glucose concentration. Therefore, we administered ^{18}F-Alfatide II first for the dual tracer imaging, and ^{18}F-FDG was injected later. In general, a higher dose of the second tracer is needed for dual tracer imaging, since it makes the signal of the second tracer stronger and less affected by the first one, which benefits parameters estimation. A 1:3 ratio between the first tracer and the second tracer has been suggested in a ^{62}Cu-PTSM and ^{62}Cu-ATSM dual tracer simulation study (17). In this study, about equivalent dose of ^{18}F-Alfatide II and ^{18}F-FDG were used, since the tumor uptake of ^{18}F-FDG is much higher than that

of ^{18}F-Alfatide II (2–4 fold). In our previous study of ^{18}F-labeled dimeric RGD peptides, tumor uptake reached equilibrium after 30 min p.i. (19); thus we chose 40 min for the injection time separation in the current study.

We validated signal recovery of the ^{18}F-FDG from the overlapped dual tracer imaging data by performing ^{18}F-FDG single tracer imaging on the same mice on the day prior to the dual tracer imaging. The reproducibility of ^{18}F-FDG has been confirmed in mouse tumor xenografts with 6 h intervals (29). We also compared the imaging results from different days and excellent reproducibility was found (Supplementary Figure 3). Consequently, to simply the situation, we ignored the change of tumor FDG uptake at a time interval of 24 h. The tumor uptake and influx rate of ^{18}F-FDG both showed good correlations between the single tracer imaging and dual tracer imaging, and the kinetic parameters calculated from the recovered FDG signal appeared to be able to reflect the real FDG accumulation.

It has been reported that doxorubicin could cause reduced tumor metabolism and angiogenesis (30–33). Based on the static image quantification, no significant differences in tumor uptake of ^{18}F-Alfatide II and ^{18}F-FDG were found after doxorubicin treatment, most possibly due to the relatively large inter-group variance and altered tumor microenvironment contributing to non-specific tumor uptake (19). Besides its definition as k_3/k_4, Bp value is also known as the ratio of B_{max} and K_d, in which B_{max} refers to the total number of receptors and K_d represents the affinity of any single receptor (34). After doxorubicin treatment, the reduced integrin $\alpha_v\beta_3$ receptor density (B_{max}) resulted in a significant decrease of the Bp value ($P < 0.01$). The FDG influx rate showed decreased value upon treatment in both control and treated group, but was more pronounced in the treated group ($P < 0.05$). The variance of the ^{18}F-Alfatide II Bp value was more significant than that of FDG influx rate, indicating more changes in tumor angiogenesis than metabolism upon doxorubicin treatment. Similar findings were also confirmed in the Abraxane treatment. These results also suggest that dynamic analysis with compartmental modeling is more sensitive than the static measurement, substantiating the benefit of kinetic analysis presented in our previous study (19).

We have previously employed the left ventricle ROI to generate the input function, as there was very little myocardial uptake of RGD (19). However, this is not appropriate for ^{18}F-FDG due to the inherent high myocardial uptake. Consequently, the abdominal aorta was chosen to outline the input function for the dual tracer imaging. Arterial blood sampling wasn't performed in this study because of the technical challenge. A population-based input function (35) or one blood sample (24) at the end of dynamic imaging may be a good choice in our future studies.

To the best of our knowledge, this is the first experimental dual tracer data set to observe angiogenesis and glucose metabolism simultaneously. Based on our previous kinetics analysis of RGD peptides, an appropriate injection time separation was chosen and the signal of the second tracer was reliably recovered using compartmental modeling. Dual tracer single scan PET imaging may become a very useful method to provide more complete tumor information simultaneously.

CONCLUSIONS

In this study, we performed dual tracer dynamic imaging using staggered injections of ^{18}F-Alfatide II and ^{18}F-FDG for simultaneous observation of angiogenesis and metabolism, which serve as sensitive, early markers of tumor responses to therapy. The signal from each tracer was successfully separated with compartmental modeling. The tumor uptake values and dynamic parameters from recovered signals were validated with single tracer imaging. The dual tracer imaging was applied to monitor the tumor response to chemotherapeutics. We found that dual-tracer single-scan imaging can be used to reflect tumor response, and quantitative kinetic parameters calculated from dynamic data are more sensitive than static imaging.

Supplementary Material

Refer to Web version on PubMed Central for supplementary material.

Acknowledgments

This work was supported in part, by National Key Basic Research Program (973 Project) (2013CB733802), and by the Intramural Research Program of the National Institute of Biomedical Imaging and Bioengineering (NIBIB), National Institutes of Health (NIH).

References

1. Jones T. The imaging science of positron emission tomography. Eur J Nucl Med. 1996; 23:807–813. [PubMed: 8662121]
2. Niu G, Chen X. Apoptosis imaging: beyond annexin V. Journal of nuclear medicine : official publication, Society of Nuclear Medicine. 2010; 51:1659–1662.
3. Kubota K, Ishiwata K, Kubota R, et al. Tracer feasibility for monitoring tumor radiotherapy: a quadruple tracer study with fluorine-18-fluorodeoxyglucose or fluorine-18-fluorodeoxyuridine, L-[methyl-14C]methionine, [6-3H]thymidine, and gallium-67. Journal of nuclear medicine : official publication, Society of Nuclear Medicine. 1991; 32:2118–2123.
4. Lehtio K, Oikonen V, Gronroos T, et al. Imaging of blood flow and hypoxia in head and neck cancer: initial evaluation with [(15)O]H(2)O and [(18)F]fluoroerythronitroimidazole PET. Journal of nuclear medicine : official publication, Society of Nuclear Medicine. 2001; 42:1643–1652.
5. Tseng J, Dunnwald LK, Schubert EK, et al. 18F-FDG kinetics in locally advanced breast cancer: correlation with tumor blood flow and changes in response to neoadjuvant chemotherapy. Journal of nuclear medicine : official publication, Society of Nuclear Medicine. 2004; 45:1829–1837.
6. Sun X, Yan Y, Liu S, et al. 18F-FPPRGD2 and 18F-FDG PET of response to Abraxane therapy. Journal of nuclear medicine : official publication, Society of Nuclear Medicine. 2011; 52:140–146.
7. Yang M, Gao H, Yan Y, et al. PET imaging of early response to the tyrosine kinase inhibitor ZD4190. European journal of nuclear medicine and molecular imaging. 2011; 38:1237–1247. [PubMed: 21360246]
8. Yang M, Gao H, Sun X, et al. Multiplexed PET probes for imaging breast cancer early response to VEGF(1)(2)(1)/rGel treatment. Mol Pharm. 2011; 8:621–628. [PubMed: 21280671]
9. Liu S, Liu Z, Chen K, et al. 18F-labeled galacto and PEGylated RGD dimers for PET imaging of alphavbeta3 integrin expression. Mol Imaging Biol. 2010; 12:530–538. [PubMed: 19949981]
10. Lang L, Li W, Guo N, et al. Comparison study of [18F]FAl-NOTA-PRGD2, [18F]FPPRGD2, and [68Ga]Ga-NOTA-PRGD2 for PET imaging of U87MG tumors in mice. Bioconjugate chemistry. 2011; 22:2415–2422. [PubMed: 22026940]

11. Guo N, Lang L, Li W, et al. Quantitative analysis and comparison study of [18F]AlF-NOTA-PRGD2, [18F]FPPRGD2 and [68Ga]Ga-NOTA-PRGD2 using a reference tissue model. PloS one. 2012; 7:e37506. [PubMed: 22624041]
12. Gao H, Lang L, Guo N, et al. PET imaging of angiogenesis after myocardial infarction/reperfusion using a one-step labeled integrin-targeted tracer 18F-AlF-NOTA-PRGD2. European journal of nuclear medicine and molecular imaging. 2012; 39:683–692. [PubMed: 22274731]
13. Black NF, McJames S, Kadrmas DJ. Rapid multi-tracer PET tumor imaging with 18F-FDG and secondary shorter-lived tracers. IEEE transactions on nuclear science. 2009; 56:2750–2758. [PubMed: 20046800]
14. Black NF, McJames S, Rust TC, Kadrmas DJ. Evaluation of rapid dual-tracer (62)Cu-PTSM + (62)Cu-ATSM PET in dogs with spontaneously occurring tumors. Physics in medicine and biology. 2008; 53:217–232. [PubMed: 18182698]
15. Kearfott KJ. Feasibility of simultaneous and sequentially administered dual tracer protocols for measurement of regional cerebral haematocrit using positron emission tomography. Physics in medicine and biology. 1990; 35:249–258. [PubMed: 2315380]
16. Koeppe RA, Raffel DM, Snyder SE, Ficaro EP, Kilbourn MR, Kuhl DE. Dual-[11C]tracer single-acquisition positron emission tomography studies. Journal of cerebral blood flow and metabolism : official journal of the International Society of Cerebral Blood Flow and Metabolism. 2001; 21:1480–1492.
17. Rust TC, Kadrmas DJ. Rapid dual-tracer PTSM+ATSM PET imaging of tumour blood flow and hypoxia: a simulation study. Physics in medicine and biology. 2006; 51:61–75. [PubMed: 16357431]
18. Fakhri GE. Ready for prime time? Dual tracer PET and SPECT imaging. American journal of nuclear medicine and molecular imaging. 2012; 2:415–417. [PubMed: 23145358]
19. Guo N, Lang L, Gao H, et al. Quantitative analysis and parametric imaging of 18F-labeled monomeric and dimeric RGD peptides using compartment model. Molecular imaging and biology : MIB : the official publication of the Academy of Molecular Imaging. 2012; 14:743–752. [PubMed: 22437879]
20. Guo J, Lang L, Hu S, et al. Comparison of Three Dimeric F-AlF-NOTA-RGD Tracers. Molecular imaging and biology : MIB : the official publication of the Academy of Molecular Imaging. 2013
21. Lang L, Li W, Guo N, et al. Comparison study of [18F]FAl-NOTA-PRGD2, [18F]FPPRGD2, and [68Ga]Ga-NOTA-PRGD2 for PET imaging of U87MG tumors in mice. Bioconjugate chemistry. 2011; 22:2415–2422. [PubMed: 22026940]
22. Wu Z, Li ZB, Chen K, et al. microPET of tumor integrin alphavbeta3 expression using 18F-labeled PEGylated tetrameric RGD peptide (18F-FPRGD4). J Nucl Med. 2007; 48:1536–1544. [PubMed: 17704249]
23. Laforest R, Sharp TL, Engelbach JA, et al. Measurement of input functions in rodents: challenges and solutions. Nuclear medicine and biology. 2005; 32:679–685. [PubMed: 16243642]
24. Vriens D, de Geus-Oei LF, Oyen WJ, Visser EP. A curve-fitting approach to estimate the arterial plasma input function for the assessment of glucose metabolic rate and response to treatment. Journal of nuclear medicine : official publication, Society of Nuclear Medicine. 2009; 50:1933–1939.
25. Guo H, Renaut RA, Chen K. An input function estimation method for FDG-PET human brain studies. Nuclear medicine and biology. 2007; 34:483–492. [PubMed: 17591548]
26. Zheng X, Wen L, Yu SJ, Huang SC, Feng DD. A study of non-invasive Patlak quantification for whole-body dynamic FDG-PET studies of mice. Biomedical signal processing and control. 2012; 7:438–446. [PubMed: 22956982]
27. Huang SC, Carson RE, Hoffman EJ, Kuhl DE, Phelps ME. An investigation of a double-tracer technique for positron computerized tomography. Journal of nuclear medicine : official publication, Society of Nuclear Medicine. 1982; 23:816–822.
28. Kadrmas DJ, Rust TC, Hoffman JM. Single-scan dual-tracer FLT+FDG PET tumor characterization. Physics in medicine and biology. 2013; 58:429–449. [PubMed: 23296314]
29. Dandekar M, Tseng JR, Gambhir SS. Reproducibility of 18F-FDG microPET studies in mouse tumor xenografts. J Nucl Med. 2007; 48:602–607. [PubMed: 17401098]

30. Guo L, Fan L, Pang Z, et al. TRAIL and doxorubicin combination enhances anti-glioblastoma effect based on passive tumor targeting of liposomes. Journal of controlled release : official journal of the Controlled Release Society. 2011; 154:93–102. [PubMed: 21609741]

31. Albertsson P, Lennernas B, Norrby K. Chemotherapy and antiangiogenesis: drug-specific effects on microvessel sprouting. APMIS : acta pathologica, microbiologica, et immunologica Scandinavica. 2003; 111:995–1003.

32. Lee JH, Jang JT, Choi JS, et al. Exchange-coupled magnetic nanoparticles for efficient heat induction. Nature nanotechnology. 2011; 6:418–422.

33. Kumi Kawano YH, Iwakura Hiroshi, Akamizu Takashi, Maitani Yoshie. Combination therapy with gefitinib and doxorubicin inhibits tumor growth in transgenic mice with adrenal neuroblastoma. Cancer Medicine. 2013; 2:286–295. [PubMed: 23930205]

34. Innis RB, Cunningham VJ, Delforge J, et al. Consensus nomenclature for in vivo imaging of reversibly binding radioligands. Journal of cerebral blood flow and metabolism : official journal of the International Society of Cerebral Blood Flow and Metabolism. 2007; 27:1533–1539.

35. Eberl S, Anayat AR, Fulton RR, Hooper PK, Fulham MJ. Evaluation of two population-based input functions for quantitative neurological FDG PET studies. European journal of nuclear medicine. 1997; 24:299–304. [PubMed: 9143468]

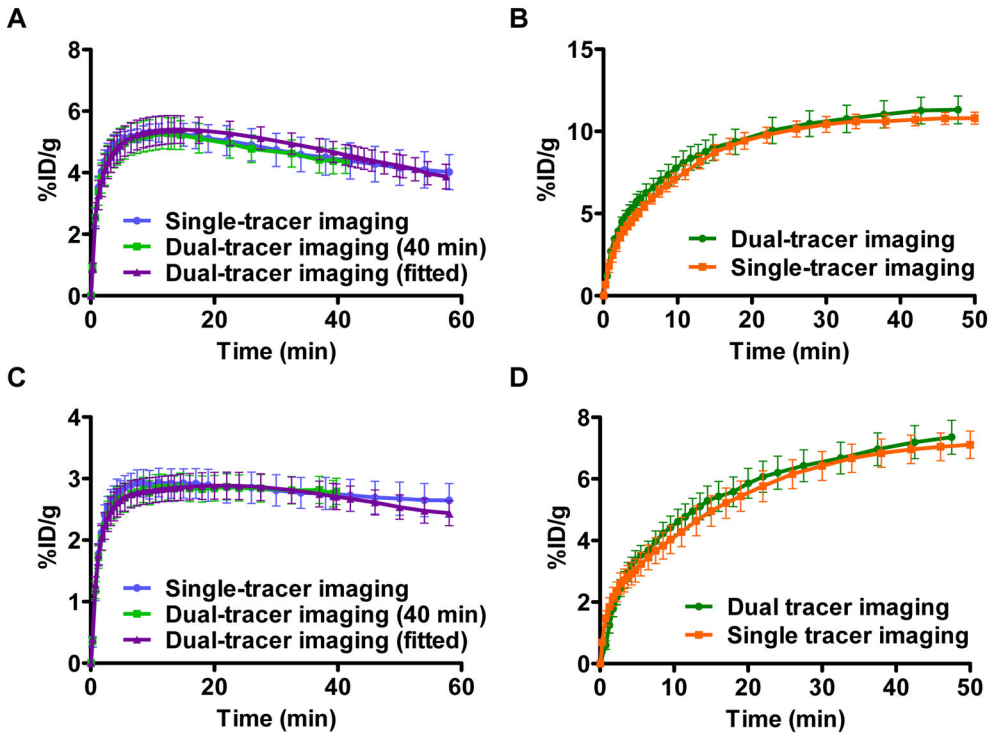

Figure 1.

(A & B) The averaged U87MG tumor uptake TACs for ^{18}F-Alfatide II (A) and for ^{18}F-FDG (B) recovered TACs in dual tracer imaging and from single tracer imaging. (C & D) The averaged MDA-MB-435 tumor uptake TACs for ^{18}F-Alfatide II (C) and for ^{18}F-FDG (D) recovered TACs in dual tracer imaging and from single tracer imaging. Tumor uptake was normalized by injection dose and expressed as %ID/g (mean ± SEM).

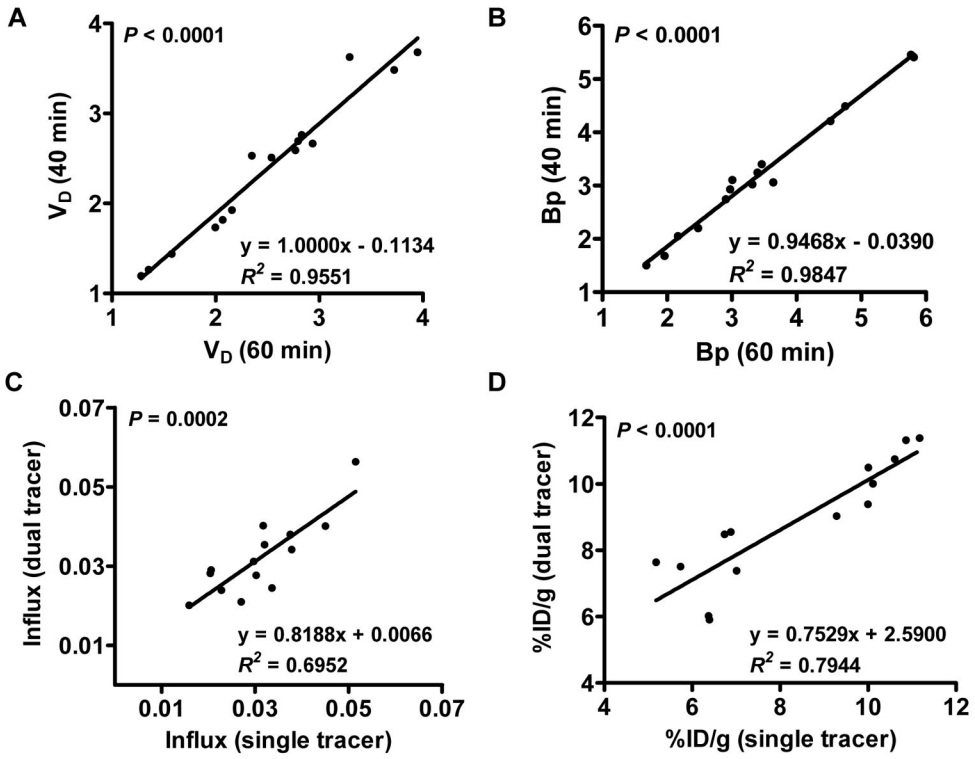

Figure 2.

(A & B) The correlation between dynamic parameters V_D and Bp calculated from 60 min and 40 min ^{18}F-Alfatide II TACs. (C & D) The correlation of ^{18}F-FDG tumor influx rate (C) and tumor uptake (D) between single and dual tracer imaging. The linear regression equation, Pearson's correlation coefficient $R^2$and the P value of linear regression F test are shown.

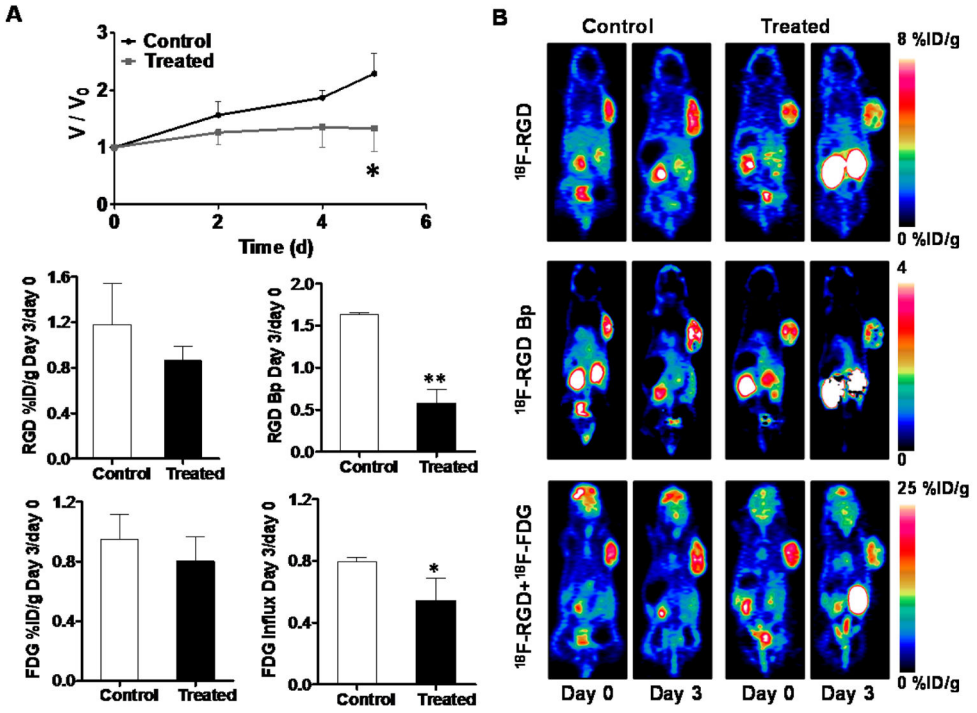

Figure 3.

(A) Relative tumor growth curves of U87MG xenografts. Doxorubicin treatment was performed on days 0 and day 2. Imaging was conducted on days 0 and day 3. (B) Representative static PET coronal images for ^{18}F-Alfatide II at 40 min (top), parametric maps of ^{18}F-Alfatide II Bp (middle), and overlapped ^{18}F-Alfatide II and ^{18}F-FDG (bottom). (C) Day-3 to day-0 ratios of static tumor uptake and dynamic parameters from ^{18}F-Alfatide II/18F-FDG dual tracer dynamic PET imaging. ^{18}F-Alfatide II tumor uptake was quantified at 40min p.i. and ^{18}F-FDG tumor uptake was recovered from TAC at 50 min p.i. of ^{18}F-FDG. Paired Student t-test was used to evaluate the differences. *, P< 0.05; **, P< 0.01.

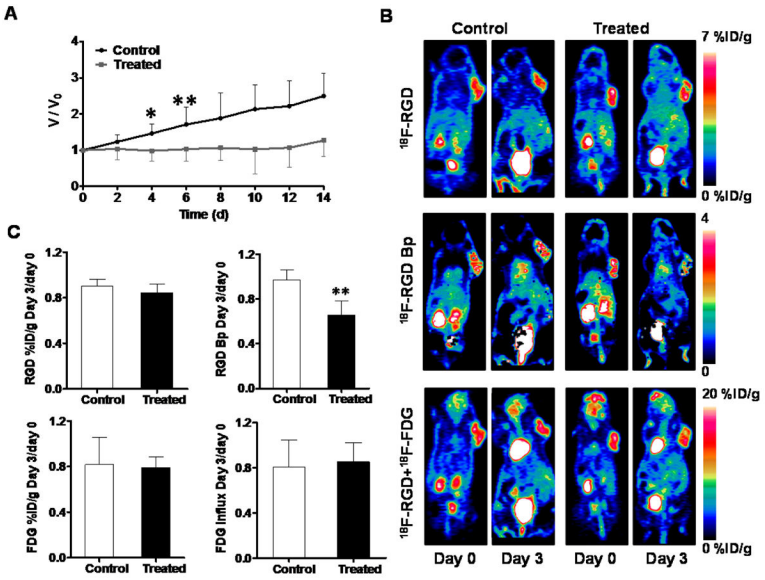

Figure 4.

(A) Relative tumor growth curves of MDA-MB-435 xenografts. Abraxane treatment was performed on days 0 and day 2. Imaging was conducted on days 0 and day 3. (B) Representative static PET coronal images for ^{18}F-Alfatide II at 40 min (top), parametric maps of ^{18}F-Alfatide II Bp (middle), and overlapped ^{18}F-Alfatide II and ^{18}F-FDG (bottom). (C) Day-3 to day-0 ratios of static tumor uptake and dynamic parameters from ^{18}F-Alfatide II/18F-FDG dual tracer dynamic PET imaging. ^{18}F-Alfatide II tumor uptake was quantified at 40min p.i. and ^{18}F-FDG tumor uptake was recovered from TAC at 50 min p.i. of ^{18}F-FDG. Paired Student t-test was used to evaluate the differences. *, P< 0.05; **, P< 0.01.

Table 1

The schematics of imaging and therapy regimen

Groups		Day 0	Day 1	Day 2	Day 3
^{18}F-Alfatide II imaging (40 min vs. 60 min) (U87MG: 7 mice; MDA-MB-435: 8 mice)					
1	(n = 15)		+		
^{18}F-FDG signal recovery validation (U87MG: 6 mice; MDA-MB-435: 8 mice)					
2	(n=15)		※	#	
Therapy monitoring (U87MG)					
3	Control (n=4)	#			#
	Treated (n=5)	#, Δ		Δ	#
Therapy monitoring (MDA-MB-435)					
4	Control (n=6)	#			#
	Treated (n=8)	#, ±		±	#

+ ^{18}F-Alfatide II imaging; ※ ^{18}F-FDG imaging; # ^{18}F-Alfatide II and ^{18}F-FDG dual tracer imaging; Δ Doxorubicin treatment; ± Abraxane treatment

Table 2

The nonlinear regression coefficient of input function and tumor TAC for each mouse

Mouse	^{18}F-Alfatide II (R^2)		^{18}F-FDG (R^2)	
	Input function	Tumor TAC	Input function	Tumor TAC
U87MG				
1	0.9984	0.9947	0.9968	0.9631
2	0.9995	0.9959	0.9969	0.9971
3	0.9993	0.9970	0.9949	0.9915
4	0.9972	0.9888	0.9950	0.9981
5	0.9977	0.9787	0.9965	0.9237
6	0.9985	0.9918	0.9863	0.9595
MDA-MB-435				
1	0.9990	0.9966	0.9846	0.9990
2	0.9989	0.9952	0.9948	0.9990
3	0.9990	0.9939	0.9794	0.9965
4	0.9987	0.9960	0.9479	0.9973
5	0.9988	0.9985	0.9947	0.9970
6	0.9991	0.9971	0.9956	0.9962
7	0.9986	0.9863	0.9949	0.9927
8	0.9944	0.9941	0.9860	0.9937

R^2, nonlinear regression correlation coefficient